Spinodal Decomposition

The NumbPies: Angela Moskal, Leandro Rizk, Sarah Rourke

December 5, 2023

1 Introduction

Spinodal decomposition is a phenomenon in materials science and physics that occurs in binary systems undergoing phase separation. This process is characterized by the spontaneous formation of compositionally distinct domains within a material, driven by thermodynamic forces seeking to minimize free energy. A key mathematical framework for describing spinodal decomposition is the Cahn-Hilliard equation, named after John W. Cahn and John E. Hilliard, who introduced it in the late 1950s [1, 2, 3]. This partial differential equation captures the dynamics of phase separation, detailing how concentration variations evolve over time. The Cahn-Hilliard equation has proven to be a powerful tool in understanding and predicting the intricate patterns that emerge during spinodal decomposition, playing a crucial role in the design and optimization of materials with tailored microstructures and properties [4, 5, 6].

2 Problem Description

The goal of this project is to numerically solve the partial differential Cahn-Hilliard equation:

$$\frac{\partial c}{\partial t} = D\nabla^2(c^3 - c - \gamma\nabla^2 c). \tag{1}$$

In the equation above, the order parameter c is dimensionless and represents the fluid concentration within the defined domain of $c \in [-1, 1]$. The diffusion coefficient, denoted by D, has units of length squared over time, while $\sqrt{\gamma}$ is the interfacial width, with units of length. The quantity in brackets, $\mu = D\nabla^2(c^3 - c - \gamma\nabla^2 c)$ is the chemical potential. This formulation is derived by extending the thermodynamic relationship that encompasses the Gibbs potential [7], providing a comprehensive understanding of the system's behavior through the interplay of concentration, diffusion, and interfacial characteristics.

To demonstrate the dynamics encoded in this equation, the fourth-order Runge-Kutta method (RK4) will be employed. Favoured for its exceptional accuracy, stability, and straightforward implementation, RK4 stands as a reliable choice for numerical solutions. The incorporation of periodic boundary conditions and consideration of the concentration domain c are important aspects in ensuring the robustness and fidelity of the solution.

In this simulation, the two mixed substances can be thought to be infinitely divisible fluids at a common and uniform density. The parameter c is therefore a measure of the predominance of the concentration of one substance with respect to the other for each gridspace.

3 Code Description

First, we populate an `N×N` matrix with concentrations sampled from a normal distribution.

```python
def gen_initial_cond(phi,N):
    '''
    Generates an NxN matrix of concentrations.
    phi = order parameter
    '''

    c0 = np.random.normal(phi,0.12,size=(N,N))

    '''Due to the nature of randomness, we don't land exactly on avg
    concentration = phi.
    Restore the desired concentration by tweaking some array values.
    '''
    c_tweak = np.copy(c0)
    C0_off = np.sum(c_tweak)/N**2 - phi
    indices = np.argwhere(np.any((c0-C0_off) < 1, axis=1))
    c_tweak[indices] -= C0_off

    return c_tweak
```
Listing 1: Generating initial condition

Then we iteratively carry out a Runge-Kutta integration of the Cahn-Hilliard equation with time step `dt`. We also have a correct_overflow function in case our update lands outside of unphysical bounds ($|c| > 1$).

```python
def rk4(X, h, derivs, *args):
    # Runge-kutta implementation
    f = derivs(X, *args)
    f1 = derivs(X + f * h/2, *args)
    f2 = derivs(X + f1 * h/2, *args)
    f3 = derivs(X + f2 * h, *args)
    f4 = X + h*(f + 2*f1 + 2*f2 + f3)/6
    return f4

def integrator(nsteps, dt, X0, derivs, *args):
    '''
    Iterates runge-kutta for nsteps of size dt starting from initial
    condition x0
    '''
    X = np.empty((nsteps + 1, N, N))
    X[0] = X0
    for i in range(nsteps):
        X[i+1] = rk4(X[i], dt, derivs, *args)
        correct_overflow(X[i+1])
    return X

def derivs(c, D, gamma):
    '''
    Accepts a 2D array of concentrations
    Calculates the time derivative of concentration using the Cahn-
    hilliard equation
    '''
    del2_c = scipy.ndimage.laplace(c, mode='wrap')  # periodic boundary
    conditions
    mu = c**3 - c - gamma * del2_c
```

```
28       dcdt = D * scipy.ndimage.laplace(mu, mode='wrap')
29       return dcdt
```

Listing 2: Functions for integrating the Cahn-Hilliard equation

Now we track the characteristic length of the spinodal structure over time using the function `track_char_lambda`. This is done by first taking a 2D Fourier transform of the N×N concentration array. Although spinodal patterns look disordered, there is a characteristic length of the domains and so the 2D Fourier transform should look like a ring. The radius of this ring in reciprocal space is related to the size of the domains in real space. We simply need to take the reciprocal of the ring radius. This function returns the characteristic length and time for each frame. We skip the first 10 time steps because early on, the N×N concentration array is still randomly populated and therefore has a characteristic length of infinity.

```
1  def track_char_lambda(ct,nsteps):
2    # Get fourier transform
3    ft = np.fft.ifftshift(ct)
4    ft = np.fft.fft2(ft)
5    ft = np.fft.fftshift(ft)
6
7    # Get array of pixel radii
8    x,y = np.meshgrid(np.arange(N),np.arange(N))
9    x0 =int(N/2)
10   y0 = int(N/2)
11   R = np.sqrt((x-x0)**2+(y-y0)**2)
12   r  = np.linspace(1,x0,num=x0)
13
14   # Iterate over all frames starting from "start"
15   start = 10
16   frames = np.arange(start,nsteps)
17   char_lambda = np.empty(nsteps-start)
18   for i in range(nsteps-start):
19     frame = frames[i]
20     fourier = np.abs(ft[frame])
21
22     # Get radial profile of fourier
23     f = lambda r : fourier[(R >= r-0.5) & (R < r+0.5)].mean()
24     intensity = np.vectorize(f)(r)
25
26     # Fit a gaussian to the radial profile
27     p0 = [194.22105802, 14.96042073, 5.09829981, 26.45927884]
28     popt, pcov = curve_fit(gauss, r, intensity,p0=p0)
29
30     # Ring radius is the center of the gaussian
31     ring_fit = popt[1]
32
33     # Convert into real space
34     char_lambda[i] = N/ring_fit
35   return frames*dt, char_lambda
```

Listing 3: Tracking the characteristic length of the spinodal pattern.

In this project, we change the initial conditions such as order parameter, diffusion coefficient and interfacial width in the functions `gen_initial_cond` and `derivs`. We then integrate them according to the Cahn-Hilliard equation using the functions in Listing 2. Finally, we see what effect the initial conditions have on the final outcome by tracking the characteristic length using the function `track_char_lambda`.

4 Results, Analysis, and Code Tests
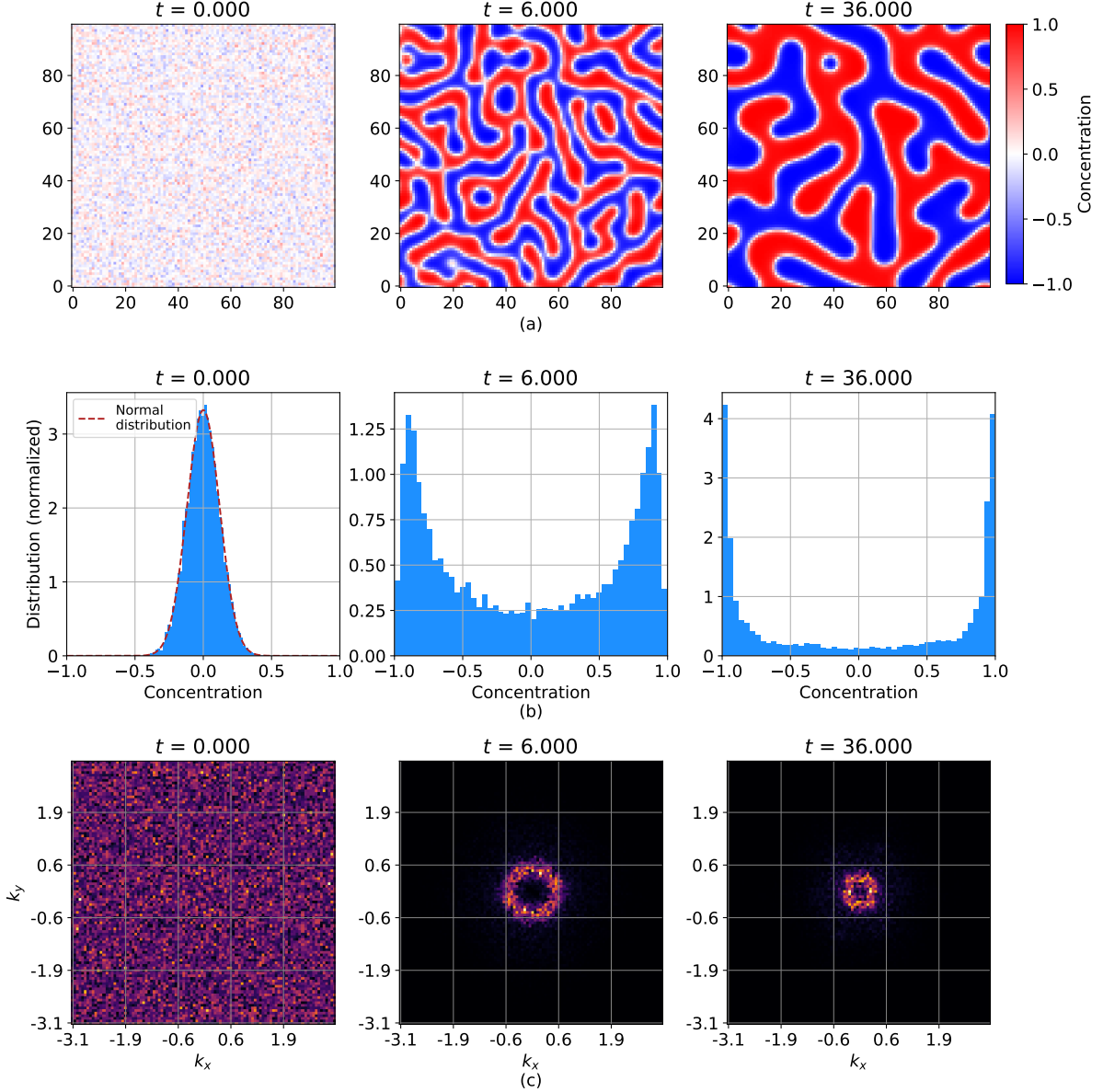
4.1 Time evolution of spinodal decomposition

Figure 1: Progression of a mixed state at $\phi_{avg} = 0$ at times $t = 0, 6.0, 35.994$. Parameters are fixed at $D = 7.0$, $\gamma = 0.8$, $\Delta t = 0.006$. **a)** Spatial distribution of order parameter for a 100×100 grid. **b)** Concentration histogram of a). **c)** 2D Fourier transform of a).

The results in Figures 1 and 2 show the evolution of spinodal decomposition over time. Videos of the simulations can be found on GitHub. Figures 1(c) and 2 demonstrate how code testing was implemented to track the characteristic wavelength to ensure it follows the expected behavior proportional to $t^{1/3}$, which will be detailed further in the Discussion section. Many other scientists have explored this numerical problem, and results are widely available online. The behaviour shown in the figures above aligned with others' previous results, which validated ours. The following sections explore the effect of the different parameters and initial conditions on the spinodal decomposition over time.
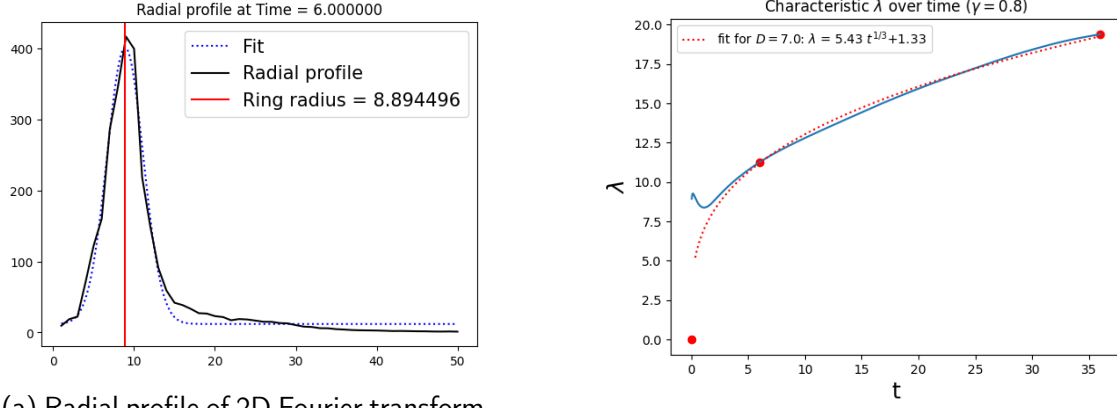
(a) Radial profile of 2D Fourier transform ring with a Gaussian fit at $t = 6.0$. The ring radius is taken to be the center of the Gaussian fit.

(b) Characteristic wavelength over time by taking the reciprocal of the 2D FT ring radius. A $t^{1/3}$ fit is provided. The times from Figure 1 are indicated by red points.

Figure 2: Extracting the characteristic wavelength of the spinodal pattern from the 2D Fourier transform and tracking it over time for a sample with $D = 7.0$, $\gamma = 0.8$ and $\Delta t = 0.006$.
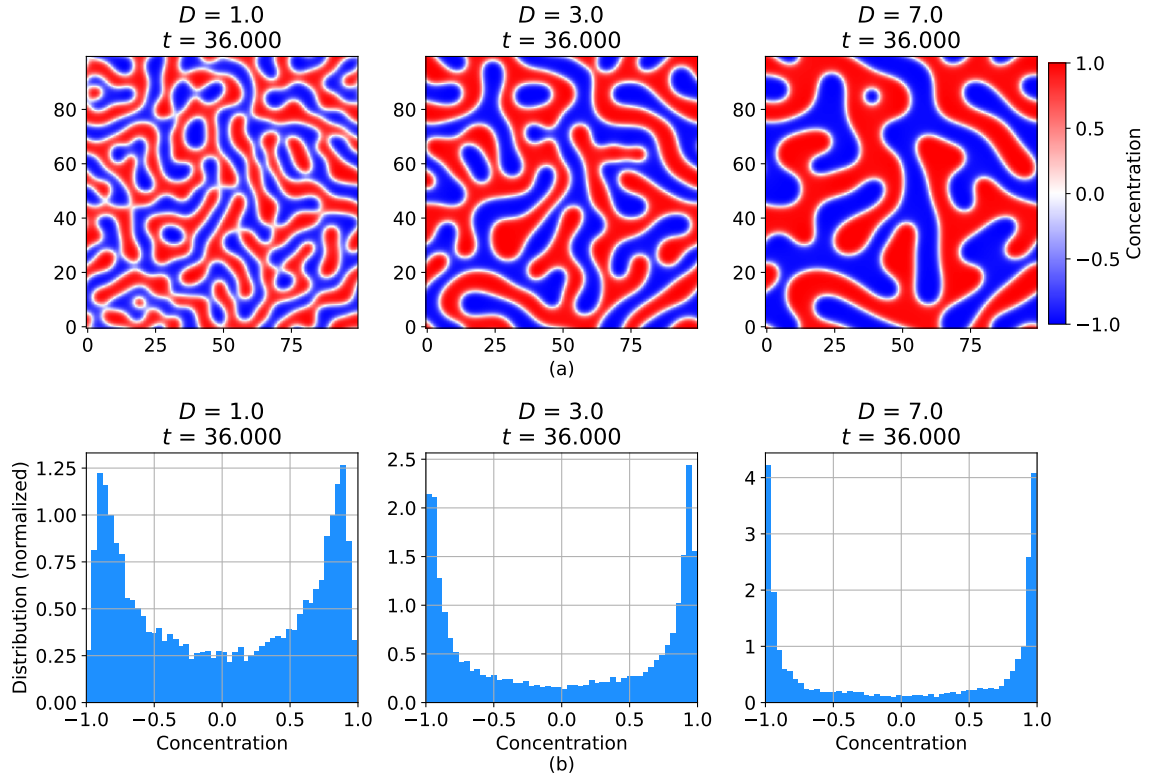
4.2 The role of the diffusion coefficient

Figure 3: Comparison of order parameter distribution for different values of D at $t = 35.999$, $\gamma = 0.8$, $\Delta t = 0.006$. **a)** Spatial distribution of order parameter for a 100×100 grid. **b)** Histogram of order parameter.

As the diffusion coefficient D increases, the rate at which the concentration field evolves intensifies, leading to larger and more pronounced patterns. This phenomenon is a consequence of faster mass transport, allowing for more extensive redistribution of components within the material. A higher diffusion coefficient promotes rapid diffusion-driven phase separation, resulting in larger characteristic wavelengths and faster growth of spinodal patterns. Conversely, a lower diffusion coefficient tends to slow down the process, leading to the formation of smaller and finer structures.

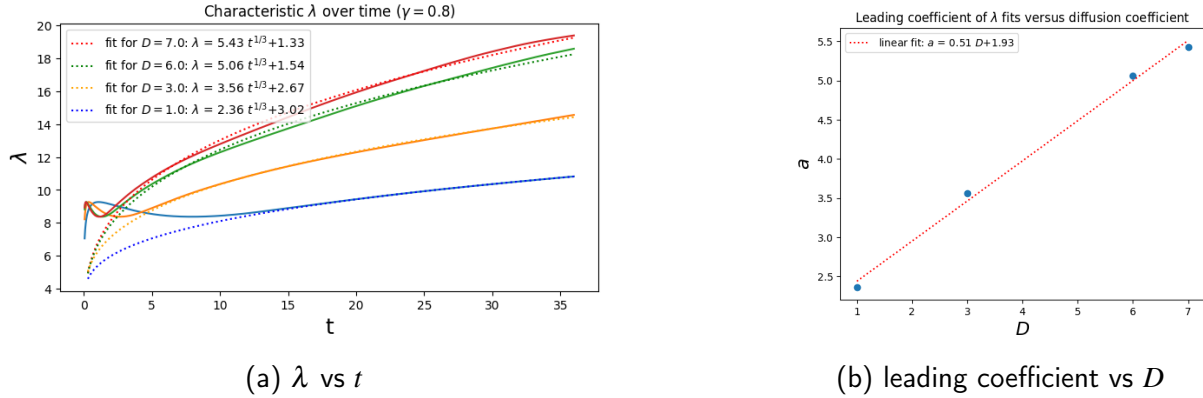(a) λ vs t (b) leading coefficient vs D

Figure 4: Dependency of characteristic wavelength on the diffusion coefficient. **a)** Characteristic wavelength tracked over time for samples with various D and $\gamma = 0.8$, $\Delta t = 0.006$. A $t^{1/3}$ fit is provided. **b)** The leading coefficients to the fits from a) are plotted against D to reveal a linear trend.

4.3 The role of the interfacial width

The parameter γ represents the square of the interfacial width and governs the rate at which the concentration field transitions between distinct phases. A smaller interfacial length results in sharper phase boundaries, leading to the formation of finer microstructures with more intricate details, as seen in Figure 5. Conversely, a larger interfacial length tends to smooth out phase transitions, promoting the development of broader and more diffuse patters. The interplay between the interfacial length and the diffusion coefficient plays a crucial role in determining the characteristic length scales and kinetics of the spinodal decomposition process.
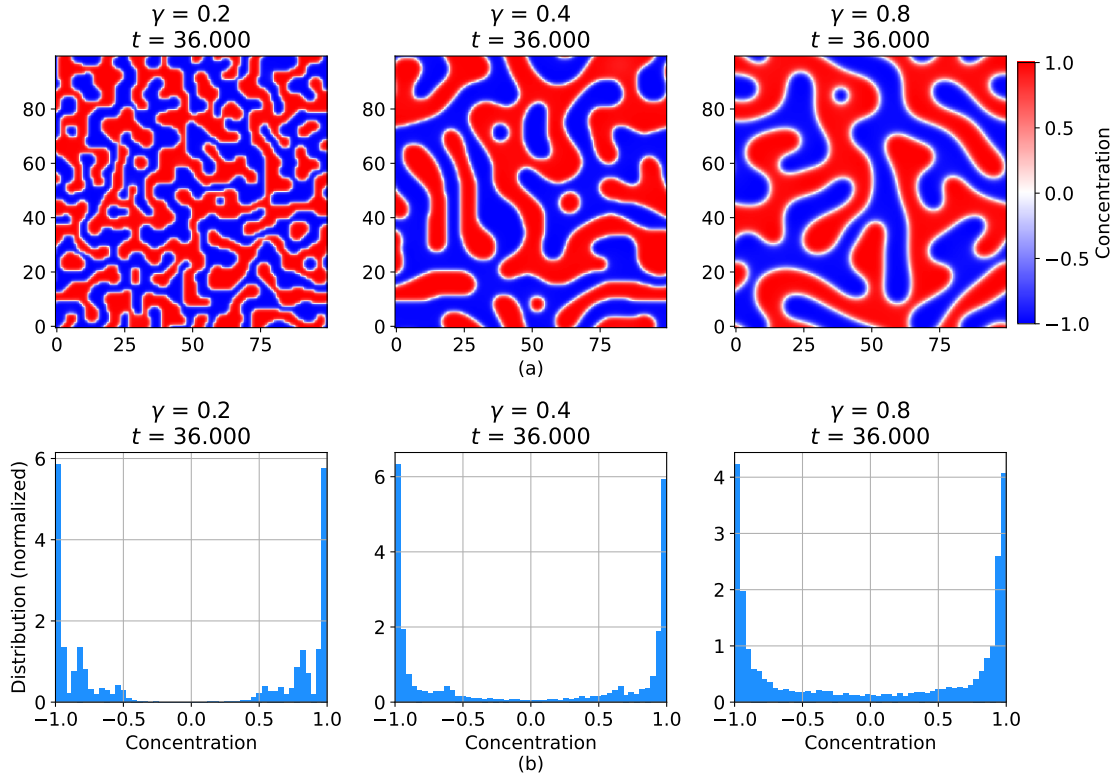
Figure 5: Comparison of order parameter distribution for different values of γ at $D = 7.0$, $\Delta t = 0.006$. **a)** Spatial distribution of order parameter for a 100×100 grid. **b)** Histogram of order parameter.

(a) λ vs t

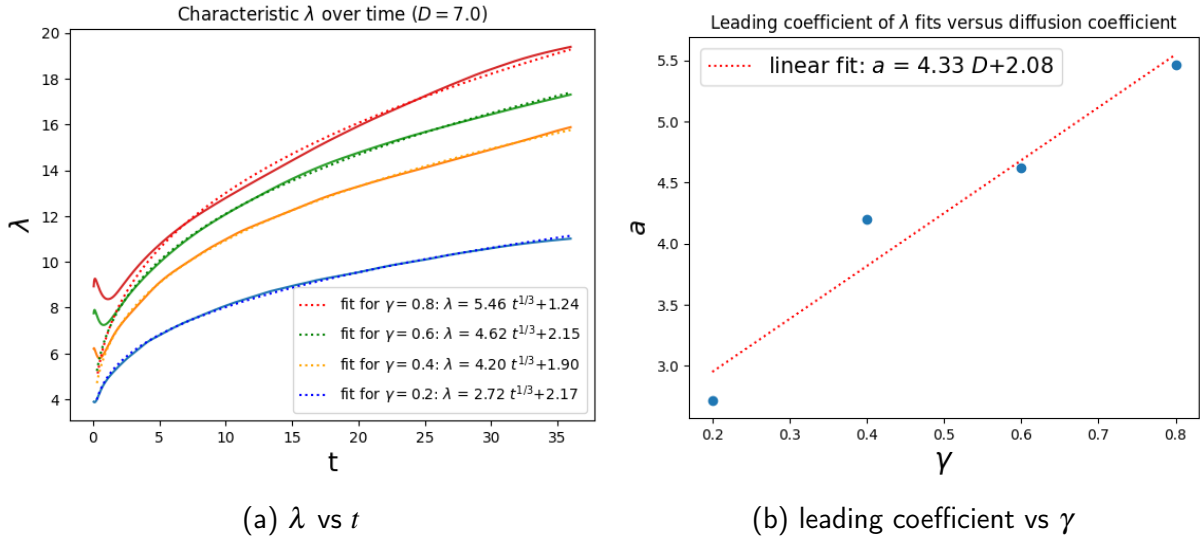(b) leading coefficient vs γ

Figure 6: Dependency of characteristic wavelength on the interfacial width. **a)** Characteristic wavelength tracked over time for samples with various interfacial widths and $D = 7.0$, $\Delta t = 0.006$. A $t^{1/3}$ fit is provided. **b)** The leading coefficients to the fits from a) are plotted against γ to reveal a linear trend.

4.4 The role of initial conditions

Now we repeat the analysis from section 4.1, except instead of starting with an equal mixture of phase A and phase B (average concentration over all space $\phi_{avg} = 0$), we start with unbalanced proportions ($\phi_{avg} = 0.2$).
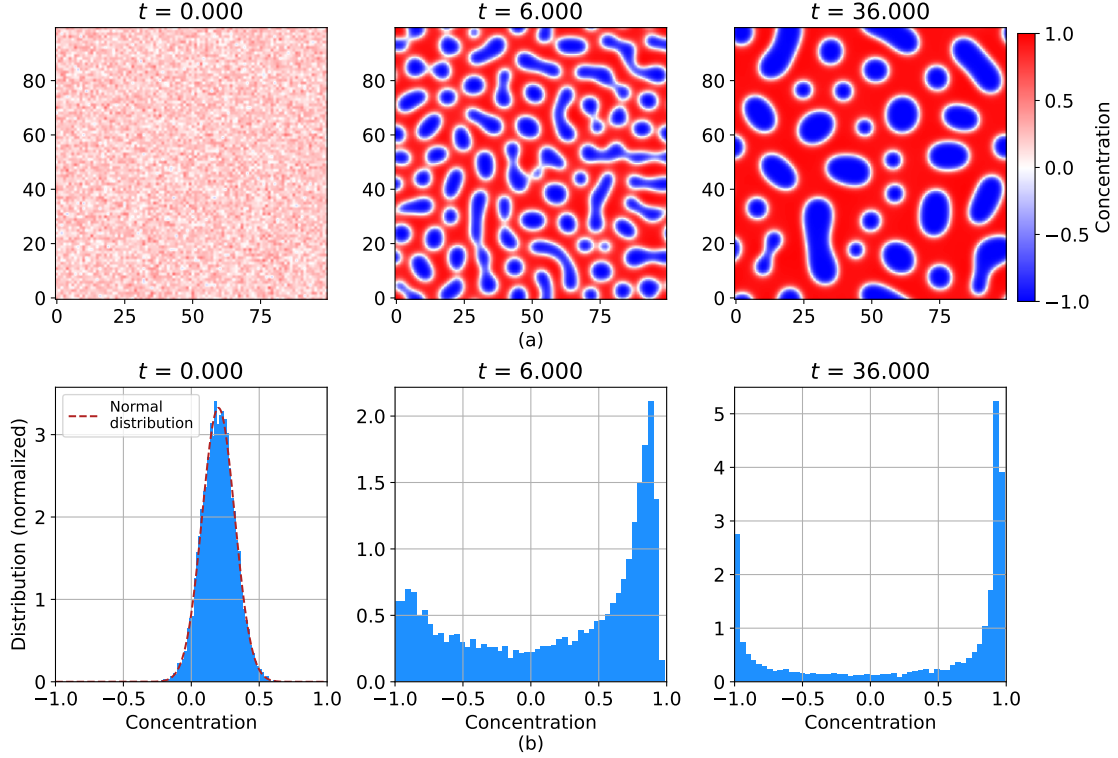

Figure 7: Progression of a mixed state with $\phi_{avg} = 0.2$ at times $t = 0, 1.2, 35.994$. Parameters are fixed at $D = 7.0$, $\gamma = 0.8$, $\Delta t = 0.006$. **a)** Spatial distribution of order parameter for a 100×100 grid. **b)** Histogram of order parameter.

Instead of a bicontinuous morphology, circular droplets start to form in a phenomenon known as Ostwald ripening [8]. The spontaneous nature of this thermodynamically-driven process arises due to the energetic preference for larger particles over smaller ones. This preference is rooted in the higher energetic stability of molecules within the interiror of a particle compared to those on its surface. The manifestation of Ostwald ripening in the simulation underscores the sensitivity of the model to nuanced phase-field parameters, offering valuable insights into the complex dynamics governing microstructure evolution.

5   Discussion and Further Improvements

The observed growth of spinodal patterns aligns with the Lifshitz-Slyozov law [9], which predicts the $t^{1/3}$ dependance. This behaviour is evident in the results at later times. However, at earlier times, when the system originates from a completely random distribution, features appear to have an infinite wavelength ($\lambda = \infty$). This characteristic arises due to the absence of discernible periodic features during the initial phase, as confirmed by the Fourier transform. Notably, the emergence of circles rather that a continuous pattern is associated with Ostwald

ripening, particularly noticeable when $\phi \neq 0$ initially.

The model exhibits sensitivity to initial conditions, especially concerning the diffusion coefficient D and interfacial width $\sqrt{\gamma}$. When these parameters are excessively large, the model experiences instability, resulting in updates that exceed reasonable bounds. Further investigations into parameter tuning and constraint implementations could enhance stability.

In future implementations, exploring adaptive integration schemes could enhance the accuracy and efficiency of the simulation. Additionally, investigating alternative integration methods beyond RK4, such as implicit methods or higher-order schemes, might provide insights into improving stability and accuracy. Conducting convergence testing, involving systematic variations in spatial and temporal discretization parameters, would further validate the accuracy of the simulation results.

6   Conclusion

In conclusion, this project addressing spinodal decomposition has yielded insightful findings and considerations. The utilization of fourth-order Runge-Kutta method for solving the Cahn-Hilliard equation proved effective, showcasing a balance between accuracy, stability, and ease of implementation. Through the simulation, we observed the manifestation of the Lifshitz-Slyozov law, evidenced by a distinct growth pattern over time. Additionally, the introduction of Ostwald ripening, leading to the formation of circular droplets, highlighted the sensitivity of the model to phase-field parameters. Further, our exploration of the diffusion coefficient and the interfacial width revealed important behaviour of microstructure formation. These insights not only enhance our understanding of the intricate dynamics involved but also pave the way for future refinements and extensions of our numerical approach.

7   Statement of Contributions

All team members contributed to all aspects of the project. Angela contributed mainly to the implementation of RK4 and the analysis of results. Leandro contributed mainly to code testing and presentation of results, including improving plots and videos. Sarah contributed mainly to the Fourier transform testing and writing of the report.

References

[1] J. W. Cahn and J. E. Hilliard, "Free energy of a nonuniform system. i. interfacial free energy," *The Journal of Chemical Physics*, vol. 28, pp. 258–267, 02 1958.

[2] J. W. Cahn, "Free energy of a nonuniform system. ii. thermodynamic basis," *The Journal of Chemical Physics*, vol. 30, pp. 1121–1124, 05 1959.

[3] J. W. Cahn and J. E. Hilliard, "Free energy of a nonuniform system. iii. nucleation in a two-component incompressible fluid," *The Journal of Chemical Physics*, vol. 31, pp. 688–699, 09 1959.

[4] P. Areias, E. Samaniego, and T. Rabczuk, "A staggered approach for the coupling of cahn–hilliard type diffusion and finite strain elasticity," *Computational Mechanics*, vol. 57, pp. 339–351, 12 2015.

[5] J. Zhu, L. Q. Chen, J. Shen, and V. Tikare, "Coarsening kinetics from a variable-mobility cahn-hilliard equation: Application of a semi-implicit fourier spectral method," *Phys. Rev. E*, vol. 60, pp. 3564–3572, 10 1999.

[6] T. Hashimoto, K. Matsuzaka, E. Moses, and A. Ōnuki, "String phase in phase-separating fluids under shear flow," *Physical Review Letters*, vol. 74, pp. 126–129, 01 1995.

[7] K. Binder, "Theory of first-order phase transitions," *Reports on Progress in Physics*, vol. 50, pp. 783–859, 07 1987.

[8] L. Ratke and P. W. Voorhees, *Growth and Coarsening*. Springer, 2002.

[9] I. M. Lifshitz and V. V. Slyozov, "The kinetics of precipitation from supersaturated solid solutions," *Journal of Physics and Chemistry of Solids*, vol. 19, p. 35–50, 04 1961.